2020

# Meeting Temporary Facility Energy Demand with Climate-Optimized Off-Grid Energy Systems

Jay F. Pearson

Torrey J. Wagner
*Air Force Institute of Technology*

Justin D. Delorit
*Air Force Institute of Technology*

Steven J. Schuldt
*Air Force Institute of Technology*



## Recommended Citation

J. Pearson, T. Wagner, J. Delorit and S. Schuldt, "Meeting Temporary Facility Energy Demand With Climate-Optimized Off-Grid Energy Systems," in IEEE Open Access Journal of Power and Energy, vol. 7, pp. 203-211, 2020, doi: 10.1109/OAJPE.2020.2998982.

This article has been accepted for publication in a future issue of this journal, but has not been fully edited. Content may change prior to final publication. Citation information: DOI 10.1109/OAJPE.2020.2998982, IEEE Open Access Journal of Power and Energy



# Meeting Temporary Facility Energy Demand with Climate-Optimized Off-Grid Energy Systems

Jay Pearson (Member IEEE), Torrey Wagner, Justin Delorit, and Steven Schuldt

***Abstract*-- Remote and contingency operations, including military and disaster-relief activities, often require the use of temporary facilities powered by inefficient diesel generators that are expensive to operate and maintain. Site planners can reduce operating costs by increasing shelter insulation and augmenting generators with photovoltaic-battery hybrid energy systems, but they must select the optimal design configuration based on the region's climate to meet the power demand at the lowest cost. To assist planners, this paper proposes an innovative, climate-optimized, hybrid energy system selection model capable of selecting the facility insulation type, solar array size, and battery backup system to minimize the annual operating cost. To demonstrate the model's capability in various climates, model performance was evaluated for applications in southwest Asia and the Caribbean. For a facility in Southwest Asia, the model reduced fuel consumption by 93% and saved $271 thousand compared to operating a diesel generator. The simulated facility in the Caribbean resulted in more significant savings, decreasing fuel consumption by 92% and saving $291 thousand. This capability is expected to support planners of remote sites in their ongoing effort to minimize fuel supply requirements and annual operating costs of temporary facilities.**

***Index Terms*--Photovoltaic cells, Microgrids, Systems engineering and theory, Optimization**

## I. Introduction

FOR military or disaster relief operations, the creation of isolated bases in remote locations are often required. These bases typically have little to no access to an established power grid and are required to generate energy for any of the base's power requirements [1]. In order to provide sustained power for the base, fuel resupply convoys are required to make frequent trips from a fuel depot to the remote location. The fuel from these convoys is then used to run multiple generator units spread throughout the base. During the Iraq and Afghan Wars, the U.S. military sustained its remote sites with daily deliveries of more than seven and a half million liters of fuel. This method of power production is extremely resource-intensive; costs not only include the purchase price of the gasoline but also in transportation, and security factors. This leads to a Fully Burdened Cost of Fuel (FBCF) that ranges from three to nearly 12 dollars per liter [2]. This leads to a significant cost when considering that diesel generators are typically run 24 hours per day, every day of the year. Using a FBCF of $4/L, the annual operational cost of the baseline generator case was $357K.

To reduce the high annual operating cost of generators, base planners have begun to incorporate the use of Hybrid Energy Systems (HES). These systems combine different energy generation technologies resulting in a more robust energy generation system. Predominantly, these systems consist of photovoltaic (PV) panels, a battery backup system, and a diesel generator [3]. Both field testing and simulation-based modeling have been used to verify the effectiveness of these systems. Field testing has proven that these technologies can be integrated into both existing power grid-connected systems and island systems [4] [5] [6]. Models have also been developed to optimize the system performance or the cost of a HES [3] [7] [8] [9] [10].

This paper is structured as follows: Section II provides a background for integrating HES systems into isolated bases as well as a background of efforts to model these interactions. Section III defines the parameters used to create the energy requirement model, while Section IV details the results of shelter analysis to minimize system component and operations cost. Section V provides a summary of the study and concluding thoughts.

## II. Literature Search

Providing fuel to geographically isolated bases is an essential element for the operation of the camp. This has become such an accepted notion that when military planners participated in wargames up until 2007, the United States Department of Defense assumed its fuel logistics were free and invulnerable [2]. Planners now include fuel logistics to include the FBCF when developing future camps. This inclusion has driven the requirement to develop technology to reduce the demand for fuel at remote bases. The response included various field tests that integrated existing products directly into shelter systems. One of the more comprehensive tests performed included evaluating different shelter insulations and thin-film PV technologies to directly offset the power demand of the shelter [4] [11]. Another demonstration explored the possibility of integrating a self-contained HES, consisting of PV panels,

This work was supported in part by the U.S. Air Force Operational Energy Office.

J. Pearson is with the Air Force Institute of Technology Department of Systems Engineering & Management (AFIT DSEM) Engineering Management Program, Wright-Patterson Air Force Base (WPAFB), OH, 45433 USA (e-mail: Jay.Pearson@afit.edu).

T. Wagner is with the AFIT DSEM Systems Engineering Program, WPAFB, OH, 45433 USA (e-mail: Torrey.Wagner@afit.edu).

S. Schuldt and J. Delorit are with the AFIT DSEM Engineering Management Program, WPAFB, OH, 45433 USA (e-mail: Steven.Schuldt@afit.edu).

This article has been accepted for publication in a future issue of this journal, but has not been fully edited. Content may change prior to final publication. Citation information: DOI 10.1109/OAJPE.2020.2998982, IEEE Open Access Journal of Power and Energy



lead-acid batteries, and a diesel generator, into a camp with moderate success [6].

To further reduce the fuel consumed at a remote base, studies sought to improve the efficiency of the Environmental Control Unit (ECU) that is commonly used to maintain interior temperatures within shelters. One study reported that as much as 80% of the energy consumed at a remote base is due to heating and cooling loads [12]. By improving an ECU's energy efficiency by 10%, one study showed that the savings in fuel costs of a large base could be as high as $2.42 million per year [13].

In addition to live demonstrations, many studies have focused on optimizing output, cost, and size of HES systems. These models range from electrifying rural areas in Algeria [7] to sizing a HES system to provide power to an Indonesian island [3]. Additionally, models have also been applied to military bases in order to increase energy resilience and cost [8], as well as evaluating the economic payback of investing in energy-saving technologies, such as LED lighting, different shelter systems, and different insulation methods [9].

Despite the significant contributions of the aforementioned research studies and demonstrations, there is no reported research that focused on: (1) analyzing the performance of single shelters; (2) computing system energy requirements based on local weather data; (3) integrating the insulative value of a structure directly into the energy requirement; (4) accounting for the insulation material's impact on cost and performance; and (5) minimizing annual operating cost by computing the optimal tradeoff between PV array size, lithium-ion energy storage capacity, diesel generator use. Accordingly, this paper demonstrates a novel model that addresses the aforementioned limitations.

## III. Method and Modeling

The present model analyzes an Alaska Small Shelter System because it is representative of the temporary facilities most frequently utilized in military and disaster-relief operations. The Alaska Small Shelter System consists of hollow aluminum segments held together by rack and pin, as shown in Figure 1. The system is placed directly on the ground with a fabric liner used as a floor. The exterior shell is made of a polyvinyl chloride-coated material 1.6mm thick [14]. All insulation for the system is placed on the interior and connected to the structural members of the shelter. The final dimensions of the tent are 9.9 m x 6.1 m x 3.1 m (L x W x H), with an exterior fabric surface area of 124 $m^2$.

Fig 1. The exterior and interior view of the modeled Alaska Small Shelter System [15].

With the intent of reducing the ECU energy requirement for a shelter system, a loading profile was chosen to simulate field conditions. The load profiles are directly related to the type of ECU used and the insulation properties of the liner used. For this model, the specifications from an HDT 60K Improved Environmental Control Unit (IECU) were used [16]. The effects of insulation are easily observed and are demonstrated in Figure 2. The uninsulated tent on the right has a higher exterior temperature, indicating an increased rate of heat loss from the shelter.

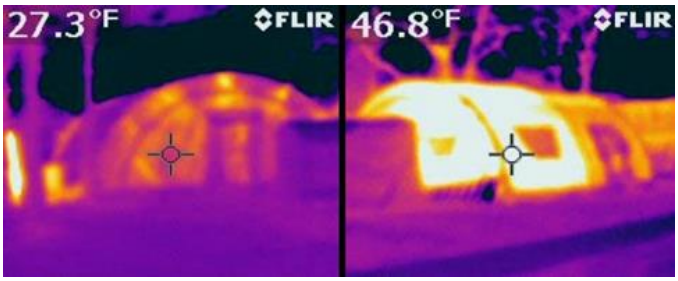


Fig. 2. The thermal profile of an insulated tent (left) against an uninsulated tent (right) [9].

The insulation properties of the shelter in this study are modeled as one-inch thick layers of material. Their corresponding insulation values are listed in Table 1. These values are used in conjunction with thermal resistivity values for exterior and interior air films as well as the shelter's exterior material.

TABLE I
Model Input Parameters

| Component | Parameter |
|---|---|
| PV system loss | 20% [8] |
| PV system efficiency | 15% [8] |
| PV capacity per $m^2$ | 106.6 W [8] |
| Li-ion Battery Allowable Depth of Discharge | 80% [21] |
| 30 kW Generator avg fuel consumption rate | 10.2 L/hour [6] |
| ECU Peak Cooling Capacity | 12.3 kW [16] |
| ECU Peak Heating Capacity | 8.8 kW [16] |
| ECU Energy Efficiency Ratio $W_{heat/cool}/W_{elec}$ | 1.69 [16] |
| Tent Material R-value $[m^2\,℃/W]$ | 0.0084 [14] |
| Fiberglass liner R-value $[m^2\,℃/W]$ | 0.60 [20] |
| Thinsulate liner R-value $[m^2\,℃/W]$ | 0.83 [13] |
| Aerogel liner R-value $[m^2\,℃/W]$ | 1.62 [13] |
| Outside Air Film R-value $[m^2\,℃/W]$ | 0.030 [22] |
| Interior Air Gap R-value $[m^2\,℃/W]$ | 0.12 [22] |

The case studies model the use of a single islanded microgrid serving all loads, whose architecture is shown in Figure 3. The architecture is then described in more detail and summarized in the operation flowchart presented in Figure 4.

This article has been accepted for publication in a future issue of this journal, but has not been fully edited. Content may change prior to final publication. Citation information: DOI 10.1109/OAJPE.2020.2998982, IEEE Open Access Journal of Power and Energy



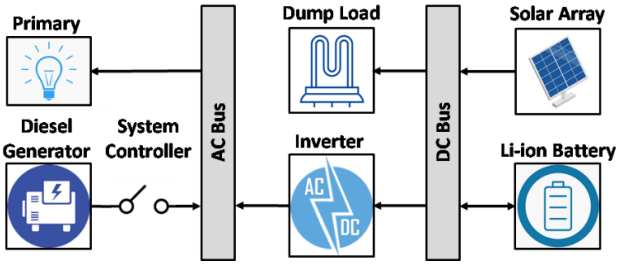


Fig 3. Systems block definition diagram model of the simulated microgrid.

The modeled operation flowchart is shown in Figure 4. Power is primarily generated through the photovoltaic solar array and is passed through an inverter to supply the alternating current primary load. Excess power generated from the solar array is stored in a lithium-ion battery, and is dissipated in a load bank if the battery is fully charged or failed. When the solar array is not able to meet the primary load, electricity is passed from the battery through the inverter to the load until fully discharged. If the battery is fully discharged and the solar array is not producing sufficient power, the system controller turns on the diesel generator to supply the deficit.

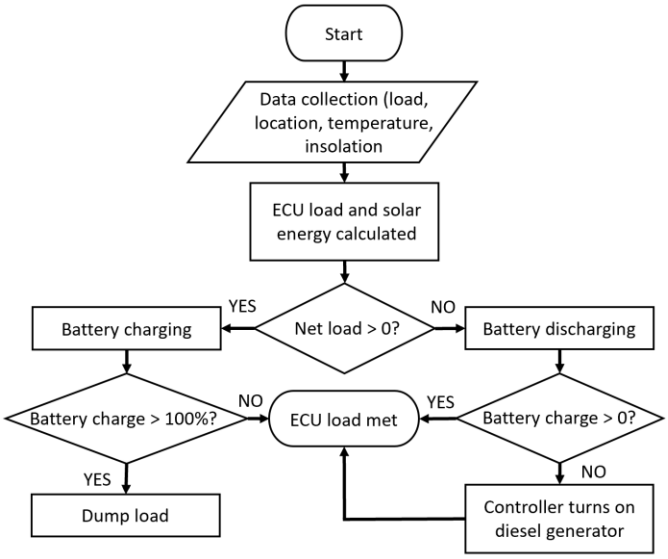


Fig 4. HES operation flowchart.

The objective of the hybrid energy system optimization model is to minimize the annual operating cost of the system. The model calculates the optimal balance between the size of the solar array, the size of the battery, the type of insulation used, and the cost associated with purchasing these components. This cost is then compared to the system's annual savings in terms of fuel cost saved.

The solar potential that can be harnessed from the system was determined using NASA's global weather data [17] [18]. 2018 Weather data, in one-hour interval periods, was used from two locations, Kabul, Afghanistan, and San Juan, Puerto Rico. These two locations were chosen to demonstrate the model's applicability in determining HES for both military applications as well as disaster relief operations. These two locations have distinctly different climates and highlight the range of solutions generated from the model. Figures 5 and 6 show the differences in the two climates in terms of their observed temperature and solar insolation levels.

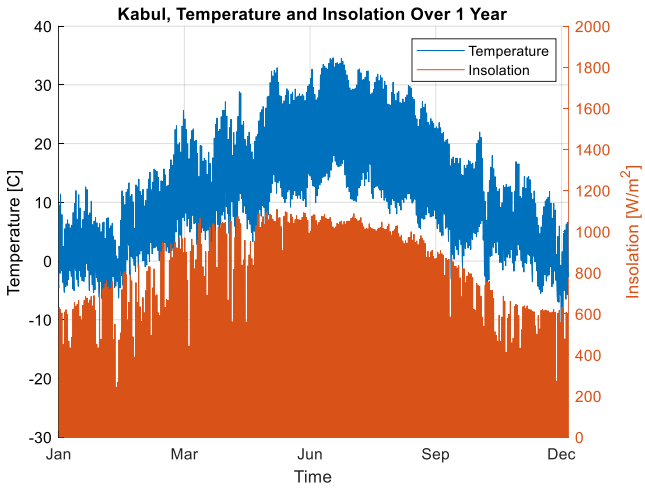


Fig. 5. Temperature (blue) and Insolation (red) data from Kabul, Afghanistan, over the course of 2018.

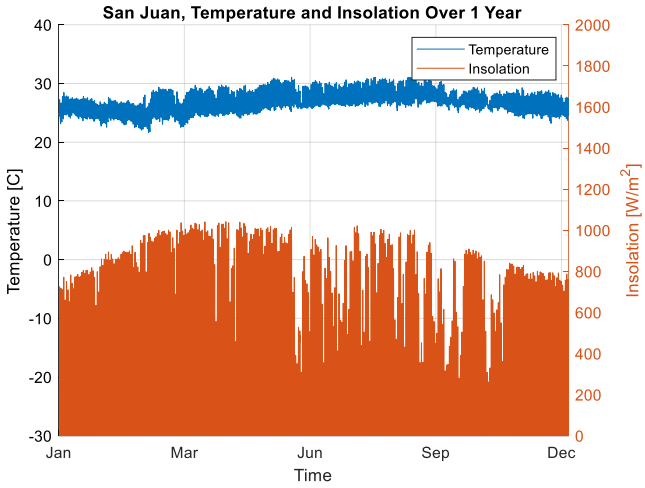


Fig. 6. Temperature (blue) and Insolation (red) data from San Juan, Puerto Rico, over the course of 2018.

To demonstrate the present model's capabilities, the MATLAB software suite was used for all system analysis. As a test case, a two-day period in late July in Kabul, Afghanistan is used to demonstrate the model's ability to predict the energy usage when there is an abundance of incoming solar radiation and large outside air temperature change. This time period demonstrates the model's behavior under peak ECU loads and provides a visual feasibility check in relation to different model variables.

The cost data utilized in the optimization model are displayed in Table II. They account for the initial cost of a PV array, the battery storage system, the cost of insulation, and the fuel costs associated with running a backup generator. The insulation costs are based on the unit cost of the material plus a historical markup factor for producing a product that is compatible with the shelter system. The table also refers to the FBCF in dollars per gallon. This term refers to the commodity price plus the total life-cycle cost of all personnel, assets, and infrastructure required to move and protect fuel from the point of sale to the end-user [3].

This article has been accepted for publication in a future issue of this journal, but has not been fully edited. Content may change prior to final publication. Citation information: DOI 10.1109/OAJPE.2020.2998982, IEEE Open Access Journal of Power and Energy



TABLE II
Cost Input Parameters

| Component | Parameter |
|---|---|
| PV array price per area [per $m^2$] | $245 [8] |
| Lithium-ion battery system [per kWh] | $400 [8] |
| Fiberglass liners [per tent] | $5,000 [20] |
| Thinsulate liners [per tent] | $6,400 [20] |
| Aerogel liners [per tent] | $64,000 [20] |
| Fully Burdened Cost of Fuel (FBCF) | $4/L [8] |

## IV. Analysis

The temperature and incoming solar radiation data from Kabul, Afghanistan, during the week of 23 July 2018, is plotted in Figure 7. It shows the large temperature swings experienced in the area, ranging from 11 to 39 degrees Celsius.

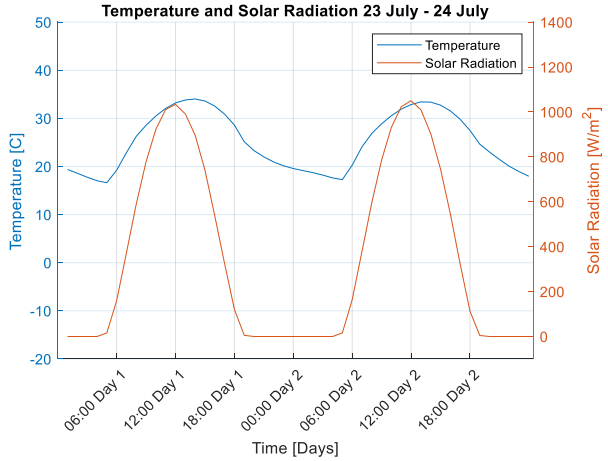


Fig. 7. Temperature and Incoming Solar Radiation profiles of Kabul, Afghanistan on 23 July 2018 – 26 July 2018 [17] [18].

From the data presented in the Net Zero Plus Joint Capability Technology Demonstration study and the specification sheet for the ECU, a linear relationship was generated empirically from comparing the outside air temperature to the power draw of the ECU at any given time [5] [16]. Using the outside temperature as an input for each iteration, a power draw for the ECU can be calculated using equation (1). This equation is used when the unit is not operating at peak capacity (Table 1) for either heating or cooling.

$$P_{ECU}\ [kW] = \frac{3 \times A_t \times |T_o - 21°C|}{\sum R_i \times \eta_{ECU} \times 1000} + 2\ kW \qquad (1)$$

Eq. 1. ECU power draw equation. $\eta_{ECU}$ represents the energy efficiency ratio of the ECU, $A_t$ $[m^2]$ is the exposed surface area of the tent, $T_o$ [°C] is the outside air temperature, R $[m^2 \cdot °C/W]$ is the summation of thermal resistances by the air films, tent material and insulation [19] [20]. 2 kW is added as a base load requirement to run the ventilation fan. The 3 is a constant to account for additional heat transfer through convection, radiation, and air infiltration [4] [5].

A conduction heat transfer model was used to account for the thermal resistive effects of the different layers between the exterior and the interior environment of the shelter. The model sums the resistive elements between the ambient temperature ($T_o$) and the interior temperature ($T_i$) to account for the changes in the heat flow of the different materials, accounting for their thickness and thermal conductive properties. Figure 8 shows the different resistive layers that are accounted for within the model.

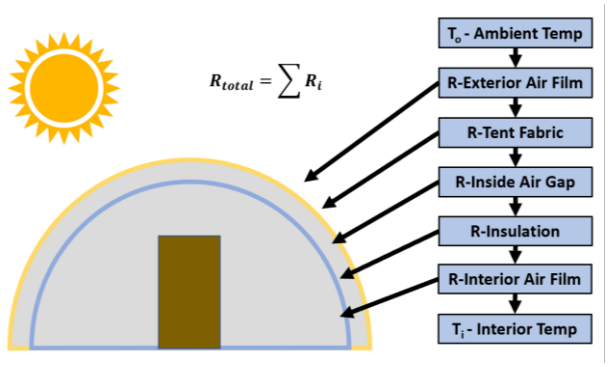


Fig. 8. Thermal Resistances affecting the heat flow from the shelter when $T_o > T_i$. When $T_o < T_i$ the heat flow (represented by the arrows) changes directions

In Figure 9, Equation 1 is plotted for the values of insulation used in this analysis, highlighting the sensitivity of power draw to the temperature set point. It is apparent that the minimal amount of power is required when the outside temperature equals the inside temperature set point of 21 °C. As the outside temperature increases or decreases away from this set point, the power required to maintain the indoor air temperature increases until it reaches the peak heating or cooling capacity of the ECU. As the figure demonstrates, the change in temperature rapidly brings an ECU connected to an uninsulated shelter to peak performance. Conversely, tents with insulative layers require a much larger temperature swing needed to bring their respective ECUs to peak heating/cooling [5] [19].

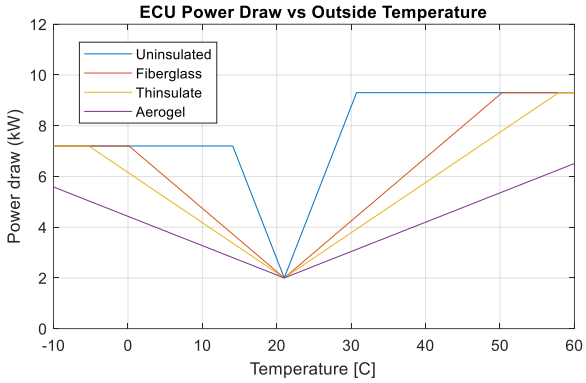


Fig. 9. ECU power draw vs. outside air temperature for various levels of insulation based on an inside air set point of 21 °C.

Figure 10 shows the resulting ECU power draw for two days of weather data when calculating the power draw from Equation 1. The figure shows there are two peak power draw times: one during the hottest time of day and the other during the coldest part of the night.

This article has been accepted for publication in a future issue of this journal, but has not been fully edited. Content may change prior to final publication. Citation information: DOI 10.1109/OAJPE.2020.2998982, IEEE Open Access Journal of Power and Energy



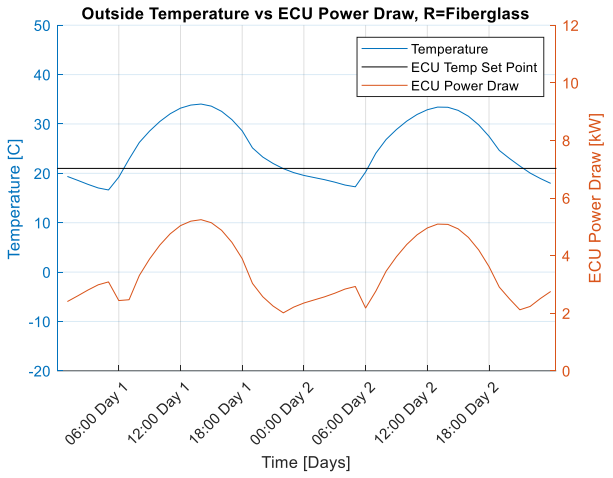


Fig. 10. Outside air temperature (blue) and the resulting ECU power draw (red) based on an inside air set point of 21 ℃ (black).

After factoring in the incoming solar radiation and converting it to useable power, then subtracting the ECU load, a load profile is generated for the net power of the system as described in (2).

$$Net\ Power\ [kW] = \left\lfloor \frac{E_e \times A_a \times \eta_{PV} \times PF}{1000} \right\rfloor - P_{ECU} \qquad (2)$$

Eq. 2. Net Power as a function of Insolation - $E_e$ [W/m$^2$], Area of the Array - $A_a$ [m$^2$], PV efficiency– $\eta_{PV}$ [%], Power factor of the entire system - $PF$ [%] and the Power draw from the ECU - $P_{ECU}$ [kW].

Net power quantifies the ability of the solar array to meet ECU demand, which is shown in Figure 11.

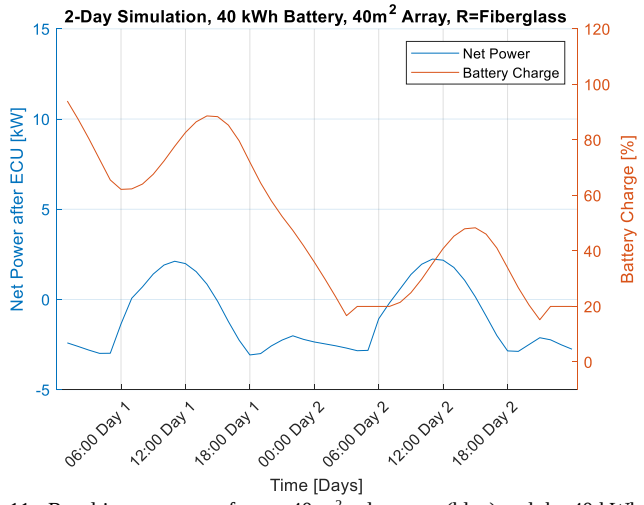


Fig. 11. Resulting net power from a 40 m$^2$ solar array (blue) and the 40 kWh battery state of charge (red).

When the net power is negative, the system drains the attached battery. The theoretical battery used in this instance has a capacity of 40 kWh and starts with a full charge. When paired with a 40 m$^2$ solar array, the battery charge is quickly depleted, and by the end of the first night, it is discharged to the allowed 80% depth of discharge (DOD). The DOD limitation is used to protect the battery and increase its service life when compared to utilizing 100% DOD [21]. To contrast this example, Figure 12 shows the same input conditions, but with a 100 m$^2$ solar array to gather solar radiation.

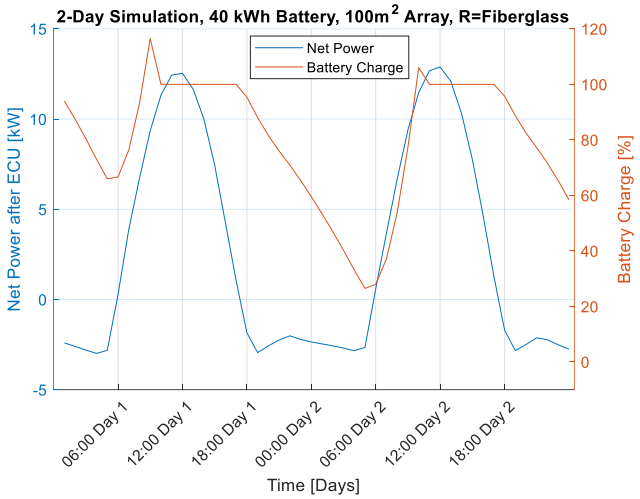


Fig. 12. Resulting net power from a 100 m$^2$ solar array (blue) and the 40 kWh battery state of charge (red).

Figure 12 illustrates that the 100 m$^2$ solar array generates more energy than can be stored by the battery. This excess energy can be quantified and used as a factor to determine a more appropriate solar array size. Another factor to consider when sizing the array is minimizing the amount of time that the battery is fully discharged. These two considerations are plotted in Figure 13 for various insulation levels.

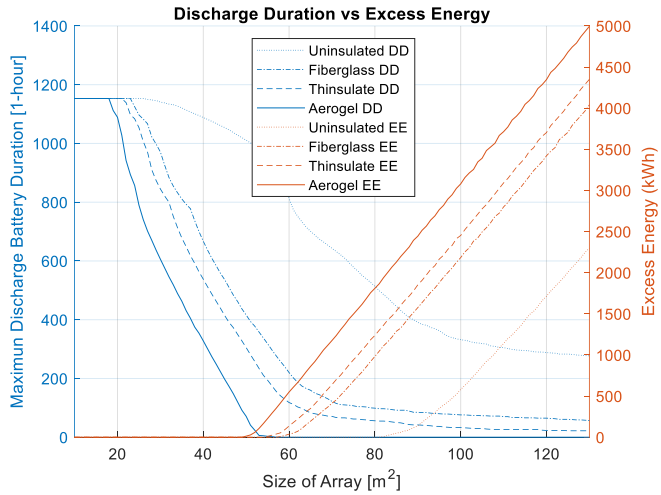


Fig. 13. Excess energy produced and the duration that the 40 kWh battery is fully discharged plotted against an increasing solar array size. The uninsulated case is represented by the dotted line, Fiberglass by the dot-dash line, Thinsulate by the dashed line, and Aerogel by the solid line.

Figure 13 indicates that for the baseline uninsulated case (dotted line), the optimal point is an array size that is approximately 95 m$^2$. This array size minimizes both the time at which the battery is fully discharged and the time when there is excess energy generated. However, for the uninsulated condition, there is a sizable amount of time where the battery is discharged regardless of the solar array size. Insulation can correct this and provide a more temperature-stable environment for living and working, by minimizing heat transfer to the outside air.

After incorporating insulation, the optimal size of the array needed is decreased to approximately 67 m$^2$ for fiberglass insulation, referencing Figure 13. This level of insulation is

This article has been accepted for publication in a future issue of this journal, but has not been fully edited. Content may change prior to final publication. Citation information: DOI 10.1109/OAJPE.2020.2998982, IEEE Open Access Journal of Power and Energy



cost-effective as a 28 $m^2$ reduction in the solar array saves $6,860 in component costs, with the fiberglass liner only costing $5,000. Similarly, the transition from a fiberglass liner to a Thinsulate liner is cost-effective, as the $1,225 savings from a 67 → 62 $m^2$ array nearly offsets the $1,400 liner price differential.

However, when the insulation level increases from Thinsulate to Aerogel, the $1,960 savings from the 62 → 54 $m^2$ solar array cannot offset the $57,600 increase in liner cost. Due to these factors, the Thinsulate liner was used for further analysis in order to determine the operating cost of the HES.

A two-dimensional sweep of configurations for the HES was performed. This included calculating the operating cost for the HES as governed by Equations (3) and (4). By calculating the cost of every combination of an array size between 1 $m^2$ and 100 $m^2$ coupled with a battery bank between 1 kWh and 100 kWh, the model is able to generate a heat map for the operating cost of the system over a time period.

$$HES\ Cost = f(A_a, kWh, R) \quad (3)$$

Eq. 3. HES Cost as a function of the Area of the array - $A_a$ [$m^2$], the size of the lithium-ion battery *kWh* [kWh], and the insulation R value used *R* [unitless].

$$Operating\ Cost = HES\ Cost + [t_{DB} \times FuelRate \times FBCF] \quad (4)$$

Eq. 4. Operating cost sums the HES cost with the cost of the fuel used by the generator, as determined by the time that the battery is discharged – $t_{DB}$ [hours], the fuel consumption rate of the generator *FuelRate* [L/hr] and the Fully Burdened Cost of Fuel *FBCF* [$].

The cost heat maps presented in Figures 15-17 are the result of the optimization process detailed in Figure 14, which accounts for component cost, one year of operation costs and the penalty cost that results from backup generator usage.

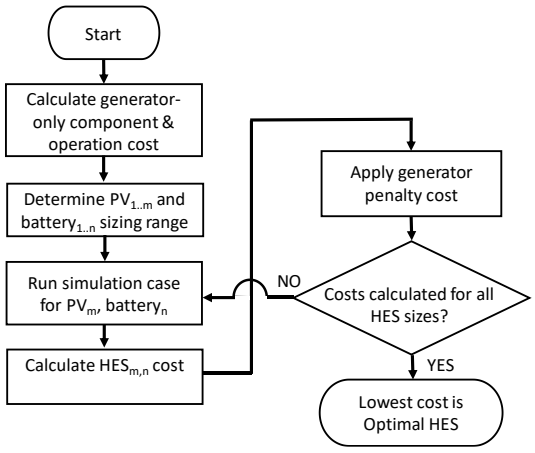


Fig 14. Optimal HES cost optimization process

As shown in Equation (4), the model also includes a cost penalty for every hour that the battery is drained, and the ECU must be run on generator power. This penalty is calculated using the FBCF of $4 per liter. Figure 15 incorporates the penalty cost and displays the cost map for the system when operating for one week.

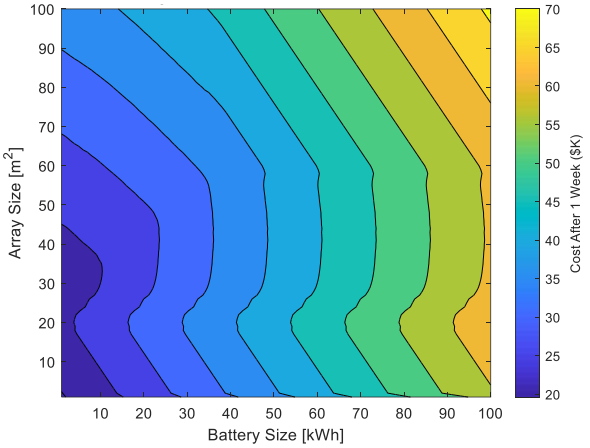


Fig. 15. Overall component and operating cost varying both solar array and battery size for Thinsulate insulation, for one week of use.

Figure 15 demonstrates that after including the cost of running a generator to make up for the time that the battery is discharged, the overall cost relationship is mostly linear and is strictly based on the size of the array and battery. The figure illustrates the optimal system in terms of cost is at point (0,0), which means that a renewable system is not cost-effective in this scenario - the baseline generator should operate the ECU.

However, when the model is simulated using weather data for the entire year, the backup generator fuel savings offset the renewable energy component costs, resulting in an optimal point. Figure 16 displays the resulting optimal system design point for Kabul, Afghanistan.

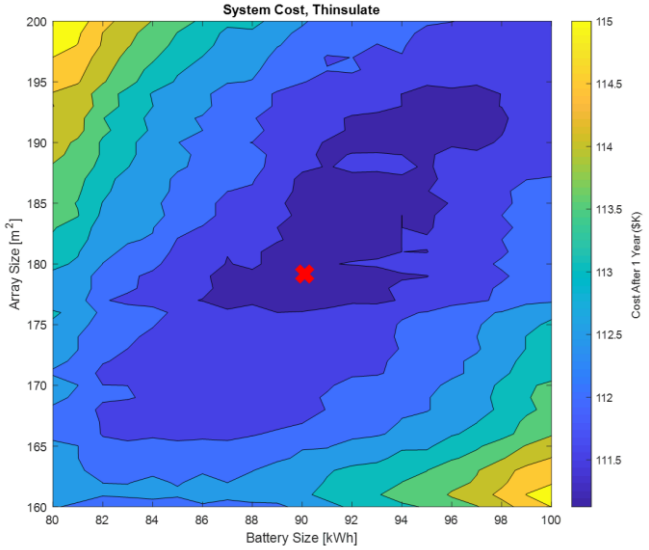


Fig. 16. Overall component and operating cost varying both the solar array and battery size for Thinsulate insulation, for one year of use in Kabul, Afghanistan.

For the one-year Thinsulate insulation scenario in Kabul, the optimal system design includes a 179 $m^2$ array (29 kW) and a 90 kWh battery. A $111,200 total operating cost was calculated by the model, including components and fuel consumed by the generator over the course of the year.

In order to contrast the result from Kabul, Afghanistan, the simulation was repeated using weather data from San Juan, Puerto Rico. This scenario resulted in the same optimal insulation (Thinsulate), and the optimal HES sizing included a

This article has been accepted for publication in a future issue of this journal, but has not been fully edited. Content may change prior to final publication. Citation information: DOI 10.1109/OAJPE.2020.2998982, IEEE Open Access Journal of Power and Energy



smaller 122 $m^2$ array (19.6 kW) connected to a 53 kWh battery. The resulting component and operating cost map is presented in Figure 17.

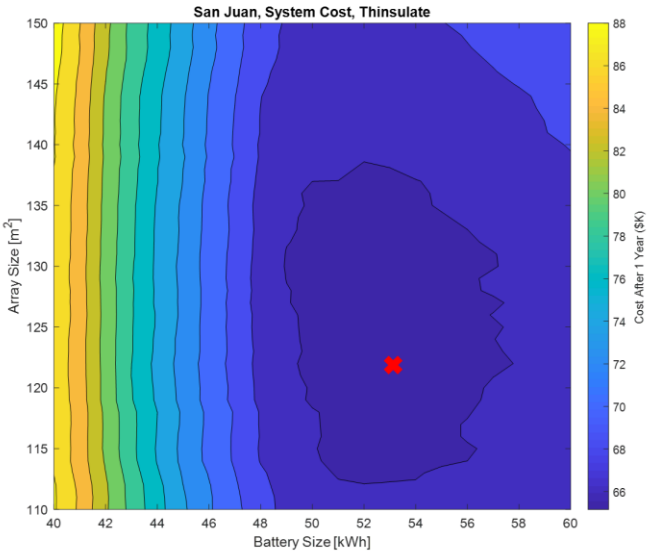


Fig. 17. Overall component and operating cost varying both the solar array and battery size for Thinsulate insulation, for one year of use in San Juan Puerto Rico.

As shown in Figure 17, a $65,160 total cost was calculated by the model, including components and fuel. The full analysis was simulated for other insulation values for both Kabul and San Juan, with their optimal design costs listed in Table III.

TABLE III
Cost Analysis Results

| | Kabul, Afghanistan | | San Juan, Puerto Rico | |
|---|---|---|---|---|
| Insulation Type | 1-Year Cost [$K] | Component Cost [$K] | 1-Year Cost [$K] | Component Cost [$K] |
| Uninsulated | 127 | 113 | 109 | 89 |
| Fiberglass | 121 | 92 | 69 | 60 |
| Thinsulate | 111 | 86 | 65 | 58 |
| Aerogel | 145 | 133 | 115 | 109 |

For Kabul, Afghanistan, optimal solutions for each insulation type had an array size that ranged from 154 $m^2$ to 257 $m^2$ with battery capacity that ranged from 77 kWh to 126 kWh. The overall optimal energy system had component costs for the solar array and battery backup system of $86,197. Over the course of one year, the fuel cost associated with running the backup generator was $25,003, which is an average of fewer than 100 minutes of operation per day. The annual operating cost of the HES system is 31.1% of the $357K baseline generator-only case.

The simulated system for San Juan, Puerto Rico, yielded even more dramatic results. Optimal systems for all insulation types had array sizes that ranged from 108 $m^2$ to 197 $m^2$, with battery systems sized between 45 kWh and 101 kWh. The lowest annual cost had a component cost of $58,000 and used only $7.7K of fuel over one year (30 minutes of average usage a day). This system resulted in an annual operating cost of 18.3%, compared to the baseline, generator only system.

## V. Conclusions

This paper presented the development of an innovative cost-performance model capable of optimizing solar array size, battery backup system, and shelter insulation type at any location. The model can minimize a shelter's component and operating cost as wells as reduce the reliance of isolated military and disaster relief sites on fuel resupply. The results of the case study analysis illustrate the unique capabilities of the model in (1) analyzing the performance of a single shelter, which allows the model to be scaled to any base size; (2) computing system energy requirements based on weather station data, ensuring the model can be adapted to any location worldwide; and (3) incorporating insulation type into energy calculations, enabling the model to consider a wide range of shelter materials. The developed model should prove useful to remote site planners, enabling them to design an optimal system to minimize the annual operating cost of fabric shelters, while incorporating site-specific climate data.

Two case studies were analyzed to demonstrate the use of the model and display its unique capabilities in selecting optimal design configurations. When using insolation, weather, and energy requirement data to optimize a shelter in Southwest Asia with Thinsulate insulation, the model generated an optimal system configuration consisting of a 179 $m^2$ solar array and a 90 kWh lithium-ion battery. When compared to a diesel generator, the modeled energy system would reduce fuel consumption by 93% and save $246 thousand within one year. Using climate data from San Juan, Puerto Rico the model's optimized system was a 122 $m^2$ array coupled with a 53 kWh battery. The HES reduced baseline fuel consumption by 92% and saved $292 thousand after one year.

A hybrid solar and battery energy system, when paired with an optimal level of shelter insulation, is a promising candidate to power ECUs in shelters for military or disaster relief operations. They provide additional energy resilience to mission essential components and reduce the amount of fuel resupply convoys needed to operate the camp.

*Authors' Note: The views and opinions of authors expressed herein do not necessarily state or reflect those of the U.S. Government or any agency thereof. Reference to specific commercial products does not constitute or imply its endorsement, recommendation, or favoring by the U.S. Government. The authors declare this is a work of the U.S. Government and is not subject to copyright protections in the United States. Additionally, the authors thank Jada Williams for expert technical assistance and for manuscript preparation. This article was cleared with case number 88ABW-2019-2426.*

## VI. References

[1] Noblis, "Sustainable Forward Operating Bases," 2010. [Online]. Available: https://www.serdp-estcp.org/content/download/8524/104509/file/FOB_Report.pdf. [Accessed 21 Oct. 2018].

[2] A. Lovins, "DoD's Energy Challenge as Strategic Opportunity," *Joint Force Quarterly*, no. 57, pp. 33-42, 2010.

[3] C. D. Rodriquez-Gallegos, O. Gandhi, D. Yang, M. Alvarez-Alvarado, W. Zhang, T. Reindl and S. K. Panda, "A Siting and Sizing Optimization Approach for PV–Battery–Diesel Hybrid Systems," *IEEE Transactions on Industry Applications* , vol. 54, no. 3, pp. 2637-2645, 2018.

[4] R. A. Fisher and M. V. Keith, "Solar Integrated Power Shelter System (SIPSS) for Basic Expeditionary Air Field Resources (BEAR)," Air Force Research Laboratory , Feb 2011. [Online]. Available: http://www.dtic.mil/dtic/tr/fulltext/u2/a542005.pdf. [Accessed 21 Oct 2018].

[5] B. Lagoon, "Net Zero Plus JCTD: Evaluation of Energy Saving Technologies for Expeditionary Shelters," US Army Natic Soldier Research, Development & Engineering Center, 4 November 2009. [Online]. Available: http://www.dtic.mil/dtic/tr/fulltext/u2/a514485.pdf. [Accessed 12 October 2018].

[6] P. B. Benasutti, W. F. Harris, M. C. Krutsch and J. A. Miletti, "Sustainability Logistics Basing-Science and Technology Objective-Demonstration; Demonstration #1-50 Person Camp Demo," U.S. Army Natick Soldier Research, Development and Engineering Center, Natick, 2017.

[7] D. Saheb-Koussa, M. Haddadi and M. Belhamel, "Economic and technical study of a hybrid system (wind-photovoltaic-diesel) for rural electrification in Algeria," *Applied Energy*, vol. 86, no. 7-8, pp. 1024-1030, 2009.

[8] T. Wagner, E. Lang, W. Assink and D. Dudis, "Photovoltaic System Optimization for an Austere Location Using Time-Series Data," in *2018 IEEE 7th World Conference on Photovoltaic Energy Conversion (WCPEC) (A Joint Conference of 45th IEEE PVSC, 28th PVSEC & 34th EU PVSEC)*, Waikoloa Village, HI, 2018.

[9] A. Rivera, "Cost Benefit Analysis of Integrated COTS Energy Related Technologies for Army's Force Provider Module," Naval Postgraduate School, Monterey, 2009.

[10] D. Chester, T. Wagner and D. Dudis, "36% Reduction in Fuel Resupply Using a Hybrid Generator & Battery System for an Austere Location," *Marine Corps Gazette*, vol. 103, no. 3, 2019.

[11] L. Biszko, "Net Zero Plue JCTD Results: Evaluation of Energy Saving Technologies for Expeditionary Shelters," 03 Oct 2011. [Online]. Available: http://www.dtic.mil/dtic/tr/fulltext/u2/a558370.pdf. [Accessed 21 Oct 2018].

[12] M. C. Ellis and R. McDevitt, "Enviromental Control Unit with Integral Thermal Storage," US Army Contracting Command - Aberdeen Proving Ground, Adelphi, 2014.

[13] P. Bulanow, P. Tabler and S. Charchan, "Expeditionary Energy Assessment: Environmental Control Unit Alternatives Study," USMC Expeditionary Energy Office, Washington DC, 2011.

[14] D. J. Murley, "Using Geographic Information Systems to Evaluate Energy Initiatives in Austere Environments," Air Force Institute of Technology , Wright-Patterson Air Force Base, 2017.

[15] H. Chris, "Army Alaska Tents," Memphite, 23 Dec 2016. [Online]. Available: https://memphite.com/YXJteSBhbGFza2EgdGVudHM/. [Accessed 3 January 2020].

[16] HDT Global, "HDT 60K IECU and S60K IECU Specifications Sheet," HDT Global, Solon, OH, 2018.

[17] S. Pfenninger and I. Staffell, "Long-term patterns of European PV output using 30 years of validated hourly reanalysis and satellite data," *Energy*, vol. 114, pp. 1251-1265, 2016.

[18] I. Staffell and S. Pfenninger, "Using Bias-Corrected Reanalysis to Simulate Current and Future Wind Power Output," *Energy*, vol. 114, pp. 1224-1239, 2016.

[19] M. N. Pilsworth , "The Calculation of Heat Loss from Tents," US Army Natick Research and Development Command, Natick, 1979.

[20] L. D. Stephenson, A. Heffron and B. B. Mehnert, "Prediction of Long Term Degradation of Insulating Materials," US Army Corps of Engineers, Engineer Research and Development Center, Champaign, 2015.

[21] J. D. Dogger, B. Roossien and F. Nieuwenhout, "Charterization of Li-Ion Batteries for Intelligent Management of Distributed Grid-Connected Storage," *IEEE Transactions and Energy Conversion* , vol. 26, no. 1, pp. 256-263, 2011.

[22] R. L. Martin, "R-Value Table," ColoradoEnergy.org, 16 July 2019. [Online]. Available: http://www.coloradoenergy.org/procorner/stuff/r-values.htm. [Accessed 4 January 2020].

## VII. BIOGRAPHIES

Jay Pearson (M'19) received the BS in Mechanical engineering from Northern Arizona University, Flagstaff, Arizona, and is pursuing an MS in Engineering Management from the Air Force Institute of Technology (AFIT), Wright Patterson Air Force Base, Ohio.

He is currently a student at AFIT in the Department of Systems Engineering & Management, and research interests include energy systems engineering.

Torrey Wagner received the BS in electrical engineering from the University of Minnesota, Minneapolis, Minnesota, the MS degree in aerospace systems engineering from Loughborough University, UK, and the PhD degree in electrical engineering from AFIT, Wright Patterson Air Force Base, Ohio.

He is currently with AFIT in the Department of Systems Engineering & Management, and research interests include agile software systems engineering and energy systems engineering.

Justin Delorit received the BS in civil engineering from Michigan Technological University, Houghton, Michigan, the MS degree in engineering management from AFIT, Wright-Patterson Air Force Base, Ohio, and the PhD degree in civil engineering from the University of Wisconsin-Madison, Madison, Wisconsin.

He is currently with AFIT in the Department of Systems Engineering & Management, and research interests include climate forecasting and asset resiliency under climate nonstationarity.

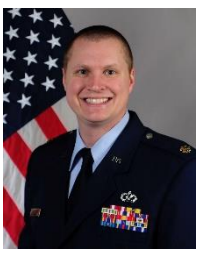

Steven Schuldt received the BS in civil engineering from the University of Illinois, Urbana-Champaign, the MS degree in environmental engineering and science from AFIT, Wright-Patterson Air Force Base, Ohio, and the PhD degree in civil engineering from the University of Illinois, Urbana-Champaign.

He is currently with AFIT in the Department of Systems Engineering & Management, and research interests include multi-objective optimization, installation resilience, and sustainability.